Comparison of *h*- and *p*-Derived Output-Based Error Estimates for Directing Anisotropic Adaptive Mesh Refinement in Three-Dimensional Inviscid Flows

Chris Ngigi, L. Freret, C. P. T. Groth

http://arrow.utias.utoronto.ca/~groth/

IHPCSS 2017
Boulder, CO, U.S.A.

June 26^{th}, 2017

Introduction and Motivation

Computational Fluid Dynamics (CFD)

- Increase in computer memory and processing power.
- CFD - capture complex phenomena. {Parallel algorithms, accuracy, computational time, costs?}
- To reduce memory & storage requirements, utilize local anisotropic block-based adaptive mesh refinement (AMR) of Freret and Groth [2015].
- AMR originally driven by physics-based criteria. Limitations in solution accuracy.

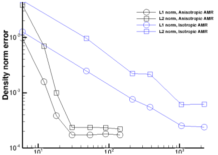

Figure 1.1: Error in the density norm for steady supersonic flow over a sphere. [Freret and Groth 2015]

Goal of this work

- Find a metric relating functional to solution error.
- Output-based error estimation for anisotropic block-based AMR .
- Benefits and associated computational cost?
- Calculate error estimates in two ways:
  - *h*-derived error estimates: via refining the mesh.
  - *p*-derived error estimates: by increasing the order of discretization.

  by reconstructing the solution, $\mathbf{U}$ and solution residual, $\mathbf{R}(\mathbf{U})$.

Euler equations

$$\frac{\partial \mathbf{U}}{\partial t} = -\left[\frac{\partial \mathbf{F}}{\partial x} + \frac{\partial \mathbf{G}}{\partial y} + \frac{\partial \mathbf{H}}{\partial z}\right] = -\mathbf{R}(\mathbf{U}) = 0,$$

- vectors **F**, **G**, **H** $\rightarrow$ inviscid flux vectors associated with the solution flux in the x, y, and z directions respectively.
- Ideal gas equation of state $p = \rho R T$ is used to close the system.

Limited 2^{nd} order FVM

$$\frac{\mathrm{d}\overline{\mathbf{U}}_{ijk}}{\mathrm{d}t} = -\frac{1}{V_{ijk}} \oint_{\partial \mathcal{V}} \vec{\mathbf{F}} \cdot \vec{n} da = \mathbf{R}_{ijk}(\overline{\mathbf{U}})$$

- Limited linear least-squares method for solution reconstruction.
- Solution space is enriched from coarse (Ω_H) to fine (Ω_h).

CENO - [Ivan and Groth 2014]

$$\frac{d\overline{\mathbf{U}}_{ijk}}{dt} = -\frac{1}{V_{ijk}} \sum_{f=1}^{N_f} \sum_{m=1}^{N_G} \left(\omega \vec{\mathbf{F}} \cdot \hat{n} A\right)_{ijk,f,m} = \overline{\mathbf{R}}_{ijk}\left(\overline{\mathbf{U}}\right)$$

- unlimited k-exact reconstruction - smooth solution.
- low-order for non-smooth content.
- Smoothness indicator used to ensure monotonicity.
- Solution space from coarse (Ω_P) to fine (Ω_p).
- store relevant num of derivatives for high-order solution.

Domain Decomposition & AMR [Freret *et al.* 2017, Freret and Groth 2015]

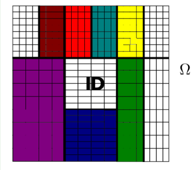

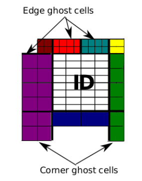

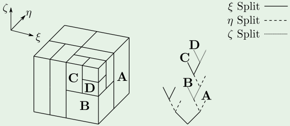

Output-Based Error Estimation - [Becker & Rannacher 1994; Giles & Pierce 2000; Venditti & Darmofal 2000]

Solve the governing equations to obtain a converged primal solution, $-\mathbf{R}(\mathbf{U}) = 0$

Define an engineering functional of interest, $J(\mathbf{U})$.

Discrete Adjoint ($\boldsymbol{\Psi}$) measures functional sensitivity to the solution residual, $\mathbf{R}(\mathbf{U})$:

$$\left(\frac{\partial \mathbf{R}}{\partial \mathbf{U}}\right)^T \boldsymbol{\Psi} = -\left(\frac{\partial J}{\partial \mathbf{U}}\right)^T$$

$\mathbf{U}_h$ is expensive to solve. Instead, approximate by $\mathbf{U}_h^H$.

The error in the functional is given in the approximation:

$$\delta J = J_h(\mathbf{U}_h^H) - J_h(\mathbf{U}_h) \approx \underbrace{(\boldsymbol{\Psi}_h^H)^T \mathbf{R}_h(\mathbf{U}_h^H)}_{\text{computable correction}} + \underbrace{(\mathbf{R_h}^{\Psi}(\boldsymbol{\Psi}_h^H))^T(\mathbf{U}_h - \mathbf{U}_h^H)}_{\text{error in computable correction}}$$

$\mathcal{E}_{K_H}$ based on CC

$$\mathcal{E}_{K_H} = \sum_{I(k)} \left\{ \left| (\boldsymbol{\Psi}_h^H)^T \mathbf{R}_h(\mathbf{U}_h^H) \right|_{I(k)} \right\}$$

$\mathcal{E}_{K_{H,P}}$ based on CC

$$\mathcal{E}_{K_{H,P}} = \left| (\boldsymbol{\Psi}_{H,p}^P)^T \mathbf{R}_{H,p}(\mathbf{U}_{H,p}^P) \right|$$

$\mathcal{E}_{K_H}$ based on ECC

$$\mathcal{E}_{K_H} = \sum_{I(k)} \left\{ \frac{1}{2} \left| \left[\mathbf{Q}_h^H \boldsymbol{\Psi}_H - \mathbf{L}_h^H \boldsymbol{\Psi}_H\right]_{I(k)}^T \left[\mathbf{R}_h(\mathbf{L}_h^H \mathbf{U}_H)\right]_{I(k)} \right| + \frac{1}{2} \left| \left[\mathbf{Q}_h^H \mathbf{U}_H - \mathbf{L}_h^H \mathbf{U}_H\right]_{I(k)}^T \left[\mathbf{R}_h^{\boldsymbol{\Psi}}(\mathbf{L}_h^H \boldsymbol{\Psi}_H)\right]_{I(k)} \right| \right\}$$

$\mathcal{E}_{K_{H,P}}$ based on ECC

$$\mathcal{E}_{K_{H,P}} = \frac{1}{2} \left| \left[\boldsymbol{\Psi}_{H,p}^P - \boldsymbol{\Psi}_{H,P}\right] \left[\mathbf{R}_{H,p}(\mathbf{U}_{H,p}^P)\right] \right| + \frac{1}{2} \left| \left[\mathbf{U}_{H,p}^P - \mathbf{U}_{H,P}\right] \left[\mathbf{R}_{H,p}^{\boldsymbol{\Psi}}(\boldsymbol{\Psi}_{H,p}^P)\right] \right|$$

Gradient-based

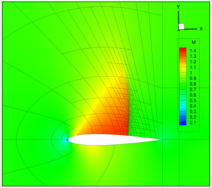

Figure 1.1: Close-up showing final gradient-based AMR mesh, 435 blocks (445,440 cells).

Output-based

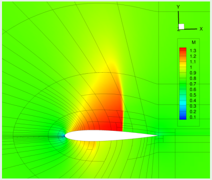

Figure 1.2: Close-up showing final output-based AMR mesh, via *p*-derived ECC-based error indicator, 259 blocks (= 265,216 cells), representing 40% cell count savings.

Functional accuracy vs. mesh size